ALONGSHORE EXTENSION OF BEACH EROSION AROUND A LARGE-SCALE STRUCTURE

TAIKI SAKASHITA[1], SHINJI SATO[1] and YOSHIMITSU TAJIMA[1]

1. *Department of Civil Engineering, The University of Tokyo, 7-3-1 Hongo, Bunkyo-ku, Tokyo, 113-8656, JAPAN. sakashita@coastal.t.u-tokyo.ac.jp, sato@civil.t.u-tokyo.ac.jp, yoshitaji@coastal.t.u-tokyo.ac.jp*

Abstract: Extensive beach erosion is observed around a large-scale structure constructed on the coast. However, the extent of the impact of coastal topographic change seems to be larger than that predicted in the past studies. In this study, the influence of large-scale structure on coastal erosion was investigated through laboratory experiments and numerical simulation. Significant extension of coastal erosion area around a large-scale structure was observed in laboratory experiments when offshore currents were superimposed and waves with alternately changing incident angles were introduced. The development of circulation currents behind the structure and the arrest of sand in the sheltered zone were considered to be the essential mechanisms for the erosion.

Introduction

Change of the movement of littoral sand drift due to a large-scale structure is one typical cause of beach erosion. It is empirically known that such coastal erosion is mainly developed in the area where the angle between the shoreline direction and the direction to the tip of the structure is smaller than 45 degrees (e.g. Sato et al, 1974). Extensive beach erosion like this pattern has been observed around large-scale structures constructed on the coast. However, many recent examples show that the erosion extends further than this '45-degree-zone'. In addition to this, since beach erosion is complexly related with many various factors such as decrease in sand supply in a watershed scale, it is very important to understand the extent of impact of large-scale structures on coastal topography change. In this study, the influence of large-scale structure on coastal erosion was investigated through laboratory experiments and numerical analysis with focuses on various factors such as variability of incident wave angles and large-scale coastal currents.

Laboratory Experiments in a Basin

Experimental Conditions and Methods

Laboratory experiments were conducted in an 11m-long and 6.5m-wide wave basin. Ground plan and cross section of the basin are shown in figure 1 The bed

slope of the basin is 1/20 in the nearshore zone and 1/10 on the offshore side. Water depth is determined as 22.5cm in order that the shoreline should be 1.1m from the onshore edge of the basin. Gray zone in Fig.1 is observed area. In this experiment, X-axis denotes the alongshore direction, and Y-axis is in the cross shore direction, and θ is the angle of wave direction defined in the anti-clockwise direction. Quartz sand with median diameter of 0.3mm was filled on the bottom of the basin to make a 4cm-thick movable bed. A breakwater was installed at 4m from left side edge of the basin. The breakwater consists of two metal panels, each length is 1m and one is situated normal to the shoreline and the other is situated obliquely with 45 degrees. Water circulation system was also arranged on both sides of the basin to generate steady coastal longshore currents with velocity as high as 10cm/s. Table 1 summarizes conditions for three experimental cases in which regular obliquely incident waves were generated for 10 hours with or without steady alongshore currents. In Case A, incident wave angle was fixed at +20 degree. Case B added artificially generated longshore currents to Case A. In Case C, the incident wave angle was alternately changed between +20 and -20 degree at every hour. For all cases, wave height in the offshore uniform depth region is 0.04m and the wave period is 1.0 second. Besides measurements of wave and current fields, measurements of bottom topography at every 3 hours were conducted by a digital camera installed above the basin.

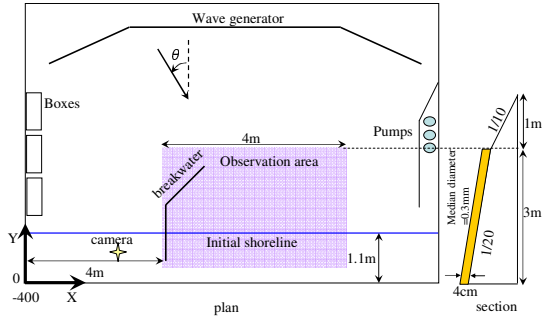

Fig. 1. Wave basin layout

In Case B, steady longshore currents were artificially generated in the basin. To genetate uniform current from left to right in Fig. 1, three pumps were installed near the right boundary of the basin. Water taken from these pumps were conveyed to left side through houses and poured in the basin through diffusers. The diffuser is made of acrylic boxes which have many small holes near the bottom, whose diameter are 1 cm. By the operation of this circulation system, 10cm/s currents were observed in the basin.

Table 1. Experiments condition

	Wave Height and Period	Wave Direction	Current
Case A (Wave Only)		20 degree	No
Case B (Wave and Current)	*H*=4cm *T*=1s	20 degree	Yes
Case C (Alternate Wave)		±20 degree	No

* In Case C, initial wave angle was 20 degree and changed between +20 and -20 degree at every hour.

In every run of experiments, shoreline position, topography change and nearshore current field were measured. Shoreline was measured every hour by manual observation at an interval of 50 cm. Topography was measured every 3 hours by using image analyzing technique. Multiple pictures were taken while the water was gradually drained and filled back in the basin. Image-rectification techniques were then applied to extract the actual coordinates of the shoreline at different water level. Then contour lines of 0cm, -2cm, -4cm, -6cm and -8cm were detected and analyzed. The accuracy of this image analysis technique was found to be smaller than 5 cm. Blue colored dye was injected behind the breakwater while generating waves and nearshore current field was observed by analyzing the sequential images that recorded the movement of the ink. Figure 2 shows an example of measurement of nearshore current field. In this photograph, the blue ink area was enhanced to be visualized easily as white color. It shows that circulation current and longshore current to the right was clearly visualized behind the breakwater.

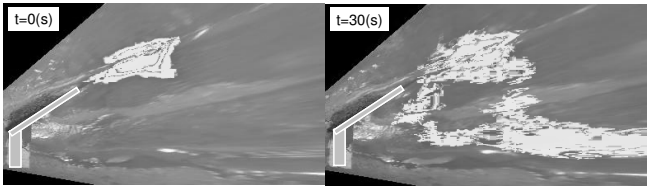

Fig. 2. An example of measurement of nearshore current (Case A, white area means inked area)

Results of Shoreline and Topography Changes

Results of shoreline and topography changes of each case will be discussed in the following. In this paper, we focus on the topography after 10 hours. Figure 3 shows the comparison of shoreline change of each case after 10 hours, and

figure 4 shows contour lines at interval of 2cm of each case after 10 hours. Dotted lines in figure 4 mean initial contour lines at an interval 2 cm depth.

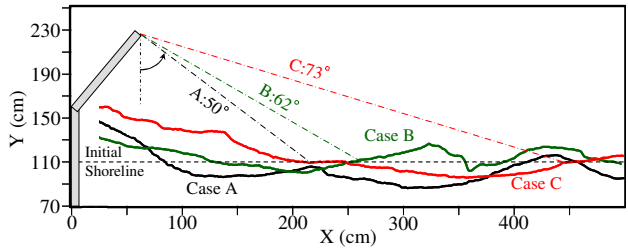

Fig. 3. Shoreline changes after 10 hours

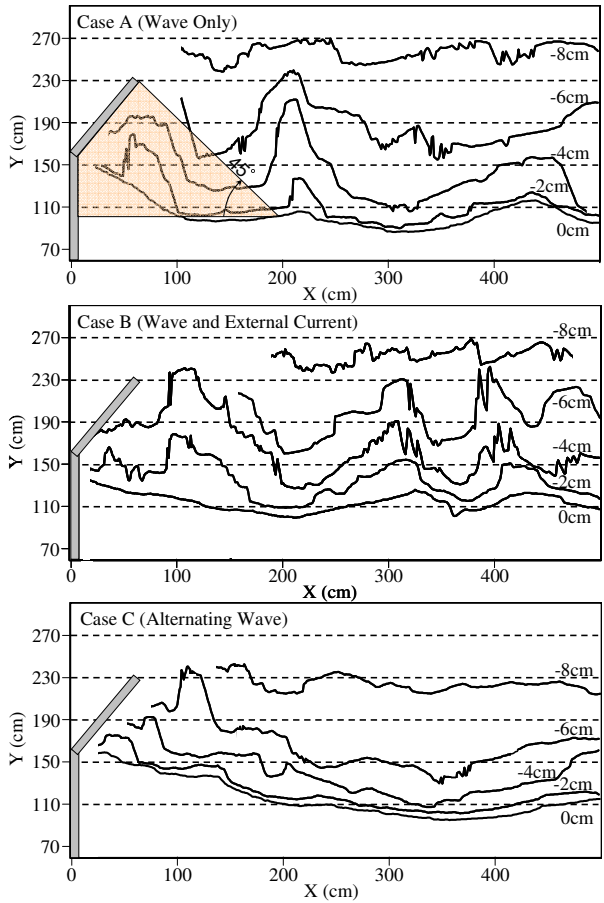

Fig. 4. Topography change for each case after 10 hours

From the results of shoreline change illustrated in figure 3, the angle of erosion area was 40 degree in Case A, 23 degree in Case B and 17 degree in Case C. Therefore the erosion area was extended in the order of A<B<C. It means that both of additional longshore currents and alternately change in incident wave angles have an influence on the extension of the erosion area. Moreover, the extension of erosion area was 20% in Case B and more than 100% in Case C compared with Case A.

Figure 4 illustrates significant differences in the erosion area as well as the shape of contour lines. The comparison between Case A and Case B shows that the accumulation, which is shown as the offshore ward movement of contour lines, in the sheltered area (shown in colored area in figure 3) can be observed in both cases, but Case B has more accumulated sands on the right hand side of the tip of the breakwater (around X=100cm) than Case A. Therefore Case B entraps more sands in the sheltered area than Case A. Moreover, in Case A, the area in which contour lines move to offshore side is X=200~220cm, on the other hand in Case B, the area is X=300cm which is farther away from the breakwater than Case A. It means that additional longshore currents could cause this difference because currents enhanced the circulation behind the breakwater. This strengthened circulation currents in Case B were also observed by the measurement of nearshore currents using blue ink.

The comparison between Case A and Case C shows that accumulation of sand in the sheltered area is observed in both cases, but the advancement of contour lines is larger in Case C than in Case A. This is considered that littoral sand drift to the breakwater side was generated when the incident wave angle was θ=-20 degree, and the sands were transported into the sheltered area and deposited there, but these sands were arrested in the sheltered area even if the wave angle changed to θ=20 degree. In addition to this, the offshoreward movement of contour lines were not observed in Case C because the circulation currents behind the breakwater were not generated when the incident wave angle was θ=-20 degree. Consequently it is considered that topography change is strongly related with nearshore current fields around the breakwater, and this will be investigated in next section by using numerical analysis.

The comparions of topographies described in the above clearly indicates that additional longshore currents have significant influence on alongshore extension of the erosion area from the comparison with Case A and Case B, and further extension of the erosion zone was also observed in Case C due to the sediment arrestment in the sheltered area of the breakwater.

Comparison of Volume of Sand Accumulated in Sheltered Area

The amount of sands accumulated in the sheltered area was calculated from the rebuilt topography data by interpolating contour lines and the difference in the volume between the initial topography and the topography after 10 hours was computed. Figure 5 shows the comparisons of the amount of sand in sheltered area.

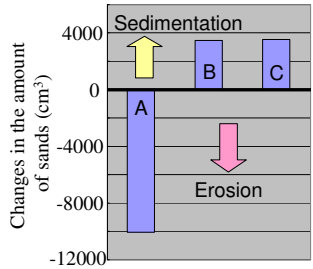

Fig. 5. Changes in the amount of sands in sheltered area between initial moment and after 10 hours.

Figure 5 shows that severe erosion is observed in Case A while accumulation is developed in Case B and Case C. Both of additional external currents and alternate change of incident wave angle could be effective to accelerate entrapment of sands in the sheltered area. The sands entrapped in the sheltered area were originated from the area of X>0 and the change of circulation currents behind the breakwater might increase the volume of littoral sand drift to left hand side. Detailed investigation for this will be tried in next section of numerical analysis.

Numerical Analysis by Shoreline Change Model

In order to confirm the physical mechanisms observed in laboratory experiments, numerical analysis of beach deformation around a structure was made based on the shoreline change model concept.

Firstly, the wave field was calculated by the time-dependent mild slope equation (Watanabe and Maruyama 1986) which could consider nearshore wave deformation including diffraction, refraction and breaking. Nearshore currents in every mesh point were then computed based on the radiation stress field calculated from the wave field. Figure 6 shows wave height and nearshore current field of three cases used in the experiments. It is confirmed that the circulation currents are enhanced in Case B in the area sheltered by the breakwater. It is also illustrated that the longshore currents due to waves with -20 degrees are decelerated in the sheltered area. It is therefore suggested that the

change in nearshore currents plays an essential role in the entrapment of sediments.

Lastly, the sediment transport rate was calculated based on these wave and currents field. The shoreline changes were calculated from longshore transport rates estimated either by Ozasa and Brampton model (1980) or by local sediment transport model (Shimizu et al., 1994). The former model calculates shoreline change by sediment transport rate modeled by the longshore distributions of wave heights and directions at breaking points. On the other hand the latter model calculates local sediment transport rates from bottom shear stress and nearshore currents.

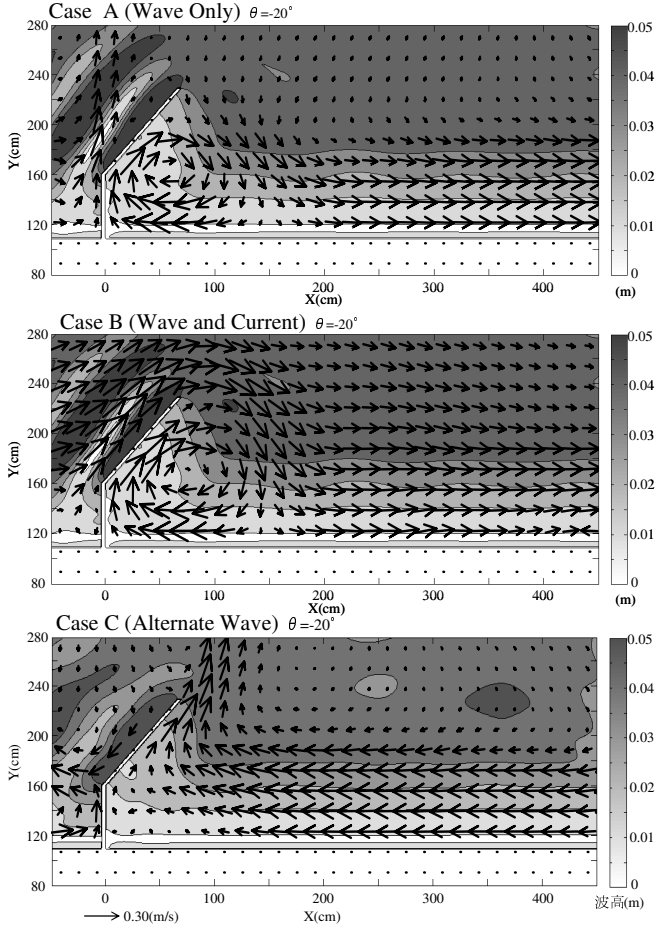

Fig. 6. Computed wave height and current fields.

Computation by Ozasa and Brampton model

The shoreline change in 10 hours was computed by Ozasa Brampton (1980) model. This model is very practical and widely applicable to compute the shoreline change around structures by considering wave diffraction and generation of nearshore currents. The longshore sand transport rate is calculated by the following equation: Eq.1.

$$I = (Ec_g)_B \left(K_1 \sin\alpha_B \cos\alpha_B - \frac{K_2}{\tan\beta} \cos\alpha_B \frac{\partial H_B}{\partial y} \right) \tag{1}$$

where K_1, and K_2 are dimensionless coefficients, tanβ is the bottom slope, α_B is the wave angle at the breaking point, H_B is wave height at breaking points and I is the longshore sand transport rate expressed in underwater weight as shown in Eq.2.

$$I = (\rho_s - \rho) g (1 - \lambda_v) Q \tag{2}$$

where ρ_s is the density of sand (=2.65(g/cm^3)), ρ is the density of water (=1.0(g/cm^3)), and λ_v is the porosity of sand (= 0.4). For the value of K_1, 0.77 is often used, but this value is based on the field data and could be changed for experimental data. In this study, the value of 0.077 was used considering matching with experimental data. The coefficient K_2 means the relative strength between circulation currents and alongshore currents which is determined at K_2 =K_1/1.5.

Computed shoreline after 10 hours by using the Ozasa Brampton model is shown in figure 7. This result is based on the wave fields generated from initial topography and on the assumption that they do not change even if the topography changed. However, the relative changes of breaker angle due to the shoreline changes were considered in this calculation.

It is confirmed in figure 7 that the accretion in the sheltered area is significant in Case C compared with those of Case A and B. At the same time, severe erosion is observed in the area farther than the location of X=80cm in Case C.

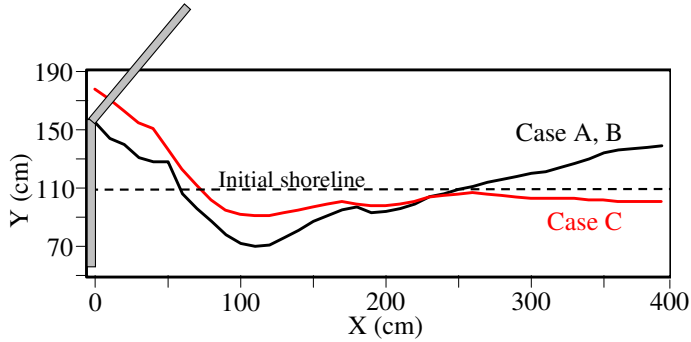

Fig. 7. Computed shorelines after 10hours with Ozasa and Brampton model (θ=20 deg.)

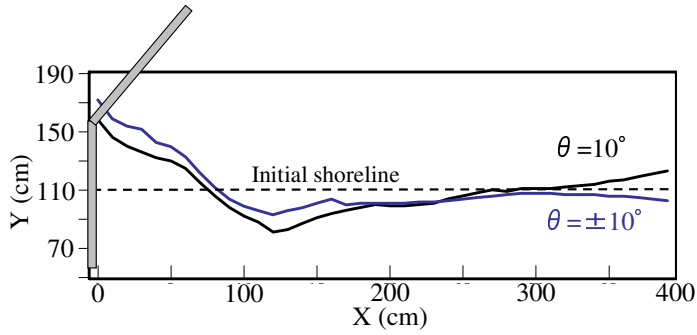

Fig. 8. Computed shorelines after 10hours with Ozasa and Brampton model (θ=10 deg.)

Additional case of the incident wave angle was 10 degree was also calculated in this model as shown in figure 8. From these results, erosion area was a little bit of enlarged compared with the wave angle was 20 degree. This is because the shoreline direction got mild to be perpendicular with the wave angle and the wave heights at breaking point were high due to less refraction. In case of alternate change in wave angle, erosion area was also enlarged farther just like the case of the incident wave angle was 20 degree.

Consequently, application of Ozasa and Brampton's model showed that in case of alternate change in incident wave angle erosion area was significantly extended compared with the case of constant wave angle, although the longshore component of energy flux of incident waves was zero on the average. However, as this model cannot consider the influence of additional currents (Case B), local sediment transport model was introduced in the next section in order to simulate the effects of additional longshore currents on the topograhy change.

Computation by local sediment transport model

In the 3D-SHORE model introduced by Shimizu et al.(1994), local sediment transport rate q_c due to currents was computed by the following equation (eq.3) by considering the steady states of nearshore currents field.

$$q_c = A_c(u_*^2 - u_{*c}^2)u_c / g \tag{3}$$

where u_* is the maximum bottom friction velocity, u_{*c} is the critical friction velocity corresponding for general movement of sand particles($u_{*c}^2 = \phi_c\, sgD$), ψ_c is the Shields number, g is the gravitational acceleration, D is grain diameter, u_c is current velocity, A_c is a dimensionless coefficient. The coefficient A_c was estimated from the following equation (eq.4) using sediment transport coefficient B_w.

$$A_C = 10B_w w_f \sqrt{0.5 f_w} / \left\{(1-\lambda_v)s\sqrt{sgD}\right\} \tag{4}$$

where w_f is the settling velocity of sand particles, f_w is the friction coefficient, λ_v is the porosity, s is the specific gravity of sand particle in water.

After calculating local sand transport rates in the longshore direction, total longshore sand transport rate across the surf zone was calculated by integrating them in surf zone. In this calculation, the offshore boundary of the surf zone was determined at Y=190cm on the basis of the observation of wave fields. In the sheltered area, the offshore boundary was limited by the position of the breakwater. The calculations of topography and shoreline changes were based on the assumption that the cross-shore profile of beach topography would change in parallel form as was assumed in the conventional shoreline model. Topography was renewed on the assumption of the parallel movement of contour lines at 3 and 6 hours in order to consider the change of nearshore currents and waves with beach deformation. Figure 9 shows the results of computed shoreline at 10 hours.

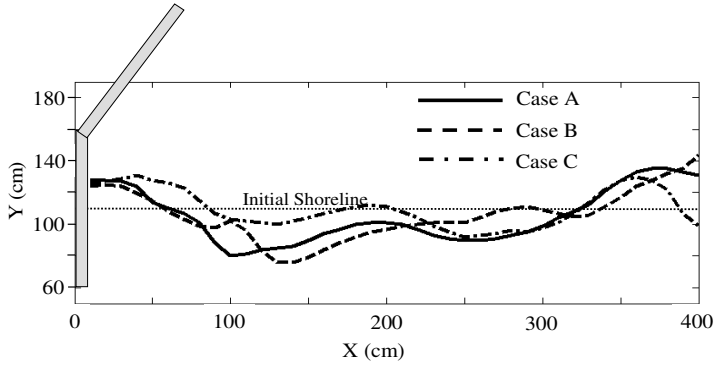

Fig. 9. Computed shorelines after 10hours with local sediment transport model

It is shown in figure 9 that the area of the severest erosion in Case B is located at X=140(cm) which is farther from the structure than that in Case A, that is X=100(cm). Therefore, it is considered that additional alongshore currents resulted in larger erosion by strengthening the circulation currents behind the breakwater as illustrated in figure 6.

From the results of distribution of littoral sand drift as illustrated in figure 10, it is also confirmed that the boundary location where moving direction of littoral sand drift changed was farther from the structure in Case B than that in Case A. This resulted in larger erosion in Case B than in Case A.

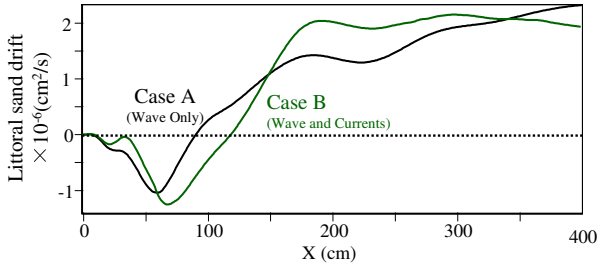

Fig. 10. Computed distribution of littoral sand drift

The shoreline advancement in the sheltered area is the largest in Case C, indicating largest amount of sand entrapment in Case C. Also the position of the severest erosion in Case C is located at X=250(cm), very far from the breakwater. It is therefore confirmed in numerical analysis that the alternate change in incident wave angle substantially increases the entrapment of sand behind a large-scale structure and enhances the beach erosion in the nearby coast.

Comparison of the amount of entrapped sand based on the local sediment transport model

The balance of amount of the sands captured in the sheltered area in 10 hours was quantitatively calculated from the topographies in the shoreline model computed with the local sediment transport model. Figure 9 illustrates the results together with experimental data.

Figure 11 demonstrates that the model simulates the loss of sand in Case A and the gain in Case C. The loss of sand in Case A is because the erosion at the downdrift end of the sheltered area is larger than the accretion in the vicinity of the breakwater. The gain of sand in Case C is considered to be due to the arrestment of sand by alternating waves.

However in Case B, the model failed to predict the gain of sand. The reason of this mismatch is considered to be due to the inadequacy of the assumption of parallel movement of contour lines introduced in the shoreline model. This can be confirmed in the results of experimental topography change (see figure 4). There is a clear difference in the bed slopes between Case A and Case B, that is, the slope of Case A is steeper than that of Case B around the sheltered area.

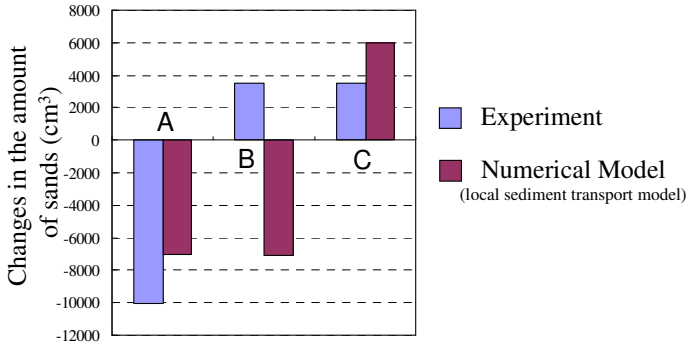

Fig. 11. Changes in the amount of captured sands after 10 hours

Therefore, it is considered that the cross shore profile change was significant in Case B, possibly due to the sand movement enhanced by the dominated circulation currents behind the breakwater. Since such three-dimensional sand movement was ignored in the numerical model, the amount of sand entrapped in the sheltered area is underestimated especially in Case B. The simulation by three-dimensional beach deformation models is remained as a future task.

Conclusions

In order to understand the mechanism of extensive erosion around large-scale coastal structures, laboratory experiments were conducted for various conditions simulating additional longshore currents and alternate change in incident wave angle. Numerical analysis based on shoreline change model was also conducted. The applicability of the numerical model was verified with the experimental results. Main conclusions are summarized as follows.

(1) The influence of the additional longshore currents and the variability in incident wave angle on the extension of beach erosion around large-scale structures was investigaetd by laboratory experiments and numerical analysis.

(2) In case of the presence of additional longshore currents, erosion area was extended by 20%. This was considered to be due to the changes in nearshore current field behind the breakwater.

(3) In case of the alternate change of incident wave angle, the erosion area was extended two times farther than the case with constant wave angle although the total longshore components of energy flux of incident waves were zero. This is because more sands were entrapped in the sheltered area than the case of constant incident wave angle.

(4) In case of the additional longshore currents or the alternately changing incident wave angle, topography changes can be computed well based on the shoreline change model by applying proper sediment transport model for each case. The extension of erosion area was simulated in both cases.

(5) A model was proposed to estimate the influence of a large-scale structure on the coast in which additional longshore currents or the seasonal variability of incident wave angle exists were introduced.

References

Sato, S., Tanaka, N., and Sasaki, K., (1974). "Coastal topography changes with the construction of Kashima Port," *Proc. Coastal Engineering Conf.*, JSCE, 21: 147-153. (in Japanese)

Tanaka, N. (1977). "Study on typical topography changes around harbors" *Proc. Coastal Engineering Conf.*, JSCE, 24: 190-194. (in Japanese)

Watanabe, A., Maruyama, K. (1986). "Numerical modeling of wave field under combined refraction, diffraction and breaking" *Coastal Engineering in Japan*, JSCE, Vol. 29: 19-39.

Ozasa, H., and A.H. Brampton, 1980. "Mathematical modeling of beaches backed by seawalls" *Coastal Engineering,* Vol. 4, 47-64.

Shimizu, T., Tsuru, M. and Watanabe, A., (1994). "Field verification of a numerical model of beach topography change due to nearshore currents, undertow and waves" *Proc. 24th Int. Conf. on Coastal Engineering*: 2610-2624.

Horikawa, K. ed., 1988. "Nearshore Dynamics and Coastal Processes" *University of Tokyo Press*., 522p.